minerals

MDPI

Article

Mineralogical Analysis of Bentonite from the ABM5 Heater Experiment at Äspö Hard Rock Laboratory, Sweden

Stephan Kaufhold [1,*], Reiner Dohrmann [1,2], Kristian Ufer [1], Daniel Svensson [3] and Patrik Sellin [3]

[1] Department of Technical Mineralogy and Clay Mineralogy, BGR—Bundesanstalt für Geowissenschaften und Rohstoffe, Stilleweg 2, D-30655 Hannover, Germany; Reiner.Dohrmann@bgr.de (R.D.); Kristian.Ufer@bgr.de (K.U.)
[2] Department of Technical Mineralogy, Sedimentology, LBEG—Landesamt für Bergbau, Energie und Geologie, Stilleweg 2, D-30655 Hannover, Germany
[3] Department of Research and Safety Assessment, SKB—Svensk Kärnbränslehantering AB, P.O. Box 5864, S-102 40 Stockholm, Sweden; Daniel.Svensson@skb.se (D.S.); patrik.sellin@skb.se (P.S.)
* Correspondence: s.kaufhold@bgr.de; Tel.: +49-511-6432765

Abstract: The present study reports on the analysis of all blocks of the ABM5 test, which is a medium scale bentonite buffer deposition test. In contrast to similar tests, the ABM5 was conducted at higher temperature (up to 250 °C). The aim of the study was to characterize the chemical and mineralogical reactions and to identify the effect of the extraordinarily high temperature. Reactions observed were similar to those observed in previous and/or similar tests covering cation exchange, anion inflow, dissolution and precipitation of C- and S-phases, Fe corrosion, and Mg increase at the heater. Neither the type nor the extent of the different reactions could be related to the significantly higher temperature. However, due to the absence of lubricant used between heater and bentonite, it could be proved that the calcite previously present was dissolved and precipitated as siderite at the contact, pointing towards the importance of the presence of carbonate when considering different Fe corrosion products. Moreover, for the first time, a decrease of the Mg content at the heater was observed, which was probably because a Mg-rich clay was used. The reasons for Mg increase or decrease are still not completely understood.

Keywords: bentonite; technical barrier; Äspö; ABM-test; smectite alteration

check for updates

Citation: Kaufhold, S.; Dohrmann, R.; Ufer, K.; Svensson, D.; Sellin, P. Mineralogical Analysis of Bentonite from the ABM5 Heater Experiment at Äspö Hard Rock Laboratory, Sweden. *Minerals* **2021**, *11*, 669. https://doi.org/10.3390/min11070669

Academic Editor: Francisco Franco

Received: 15 April 2021
Accepted: 17 June 2021
Published: 23 June 2021

Publisher's Note: MDPI stays neutral with regard to jurisdictional claims in published maps and institutional affiliations.

Copyright: © 2021 by the authors. Licensee MDPI, Basel, Switzerland. This article is an open access article distributed under the terms and conditions of the Creative Commons Attribution (CC BY) license (https://creativecommons.org/licenses/by/4.0/).

1. Introduction

Bentonite is currently investigated as a geotechnical barrier to enclose metal canisters containing high-level radioactive waste (HLRW) [1,2], particularly in combination with crystalline host rocks. Bentonites are mined worldwide. Materials from different deposits often show specific properties [3]. Bentonites are used in many different applications [4]. For each application, more suitable bentonites and less suitable ones exist. The aim of the bentonite industry is to identify the optimum bentonite for a specific application, to provide superior products compared to their competitors. Bentonite selection is commonly based on empirical tests in which specific properties of the bentonites are compared. Using bentonite as an HLRW barrier material, although tested for decades in experiments, from the point of view of the bentonite mining industry, is a new application. Well accepted quality determining parameters, therefore, do not yet exist. Kaufhold and Dohrmann [5] discussed ten parameters which could be used to compare the suitability of bentonites as an HLRW barrier material. However, to date, there is no agreement about one or more quality determining parameters. This may also result from the fact that the bentonite requirements differ amongst the different concepts. A comparison of the performance of different bentonites is therefore an interesting task.

Comparative tests can be conducted both in clay laboratories and in underground rock laboratories as medium to large scale tests. In 2006, SKB started an experiment series in

which different bentonites are compared directly [6] at Äspö Hard Rock Laboratory (HRL) with granite as host rock. Altogether, 30 blocks (rings) made of different bentonites (diameter 30 cm, diameter of central hole for the heater 10 cm, height 10 cm) were placed on each other without any protection between them. Two of the three packages were retrieved, analysed, and reported [7–15]. In 2013, three additional packages were installed, partly with different materials (e.g., saponite, a Mg-rich smectite [16]). The target temperature of the tests was 130 °C for all tests. The temperature of ABM5, however, was low at the beginning (50 °C) because of problems increasing the water pressure in the surrounding sand filter to avoid boiling at the high temperature. In 2016, the temperature was increased up to 250 °C for about six months and in 2017 ABM5 was excavated. Temperature profiles are shown in Figure 1. To date, the ABM5 is the hottest bentonite test conducted in an underground rock laboratory (URL). In the deposition hole drilled for the ABM5-test, a fracture was observed which provided some water inflow. In the installation report, it is mentioned that "most of the water seemed to come from one fracture located 0.8 m down from the floor".

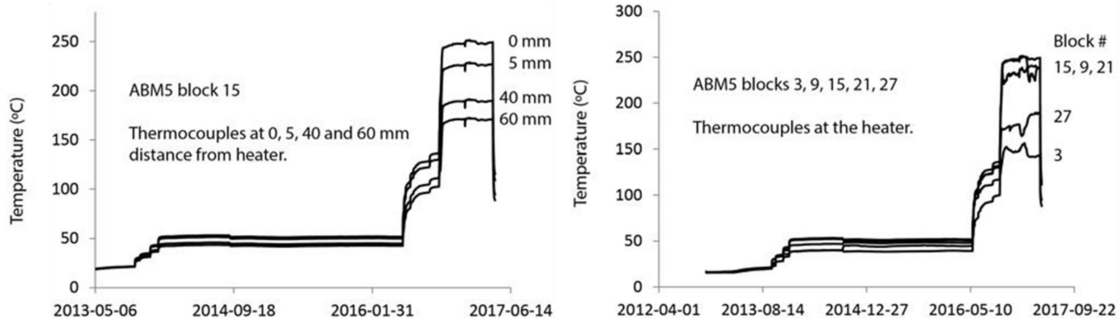

Figure 1. Temperature profiles (**left**: temperature in block 15 at different distances to the heater; **right**: temperatures at the heater of blocks 3, 9, 15, 21, 27).

The temperature reached 250 °C at the contacts of the samples to the heater, which were in the central part of the column (9, 15, 21). At the contact of the upper- and lowermost blocks to the heater, lower temperatures were observed (about 150 °C for blocks 3 and 27). In the hottest blocks (e.g., #15, Figure 1, left), more than 150 °C was reached at a distance of 6 cm from the heater.

To date, a couple of mineralogical reactions were identified in the different medium to large scale tests. In the LOT experiment, a redistribution of sulphate (gypsum, anhydrite) within the blocks was found [17,18]. The gypsum which was initially present in the bentonite was not evenly distributed after the test, but showed larger concentrations in the center of the blocks. Extensive cation exchange was observed as well [15,19]. Corrosion was observed both in case of Cu [17,20] and Fe heaters [12,13]. Corrosion products could only be found at the interface. In addition, a Mg enrichment at the contact of bentonite and metal was found in the case of both Cu [17] and Fe [11–13,21,22]. Samples with larger Mg increase showed the formation of trioctahedral phyllosilicate minerals or domains which could be detected by XRD. The mechanism behind the Mg enrichment is not yet clear [11,12,23]. In ABM1 and ABM2, organic material was found at the contact to the heater which could be explained by the lubricant (molykote) used for installation. Moreover, siderite formation was reported as well as the dissolution of cristobalite and/or clinoptilolite [12].

The aim of the present study is to characterize the mineralogical reactions that occurred in the ABM5 test and to compare them with the identified reactions. Another aim is to identify possible differences of the mineralogical reactions in terms of temperature effects, because the ABM5 test had the highest temperature yet applied in a medium- or large-scale test.

2. Materials and Methods

After dismantling the vertically installed ABM5 test in the Äspö HRL, Figeholm, Sweden, samples were collected and sent to BGR. Figure 2 illustrates the setup and dimensions

of the experiment, including the location of the sand filter and iron heater (diameter 10 cm) in the holes of the bentonite rings (diameter 30 cm, height 10 cm). The sand filter was installed to support rapid water saturation. At the beginning of the heating period, the water pressure remained unexpectedly low. In order to further support saturation, the temperature was set lower at the beginning. The temperature profile is shown in Figure 1. Experimental details can be found elsewhere [6,9,16].

Table 1. List and state of samples sent to BGR as well as samples taken at BGR from the blocks (numbers = cm distanced from heater; "x" distance to heater could not be determined). The heater was not investigated in the present study. The numbers correspond to the block numbers in ABM5. Block 1 was the lowermost block and the others were placed on top of each other.

Block no.	Material	Remark	Direction	Comment	0.1	1	5	8	x
30	MX80		30 S		√	√	√	√	
29	MX80		29 N		√	√	√	√	
28	Asha 505		28 S		√	√	√	√	
27	Calcigel	Termoelement		Fragments				√	√
26	Deponit CAN			Fragments	√	√	√	√	
25	Febex		25 W		√	√	√	√	
24	GMZ			Fragments		√	√	√	
23	Ibeco SEAL		23 W		√	√	√	√	
22	Ikosorb		22 W		√	√	√	√	
21	Kunigel V1	Termoelement		Fragments	√	√	√	√	√
20	MX80	Copper	20 W		√	√	√	√	
19	Asha NW BFL-L		19 W		√	√	√	√	
18	Rokle		18 W		√	√	√	√	
17	Saponite		17 W		√	√	√	√	
16	Asha 505	Copper	16 NW		√	√	√	√	
15	MX80	Termoelement + Titanium	15 W		√	√	√	√	
14	Rokle		14 NW		√	√	√	√	
13	Febex		13 W		√	√	√	√	
12	Saponite			Fragments	√			√	√
11	Ibeco SEAL		11 S		√	√	√	√	
10	Calcigel			Fragments	√	√	√	√	
9	Asha NW BFL-L	Termoelement	9 N	Partial	√		√		√
8	MX80		8 S		√	√	√	√	
7	Ikosorb		7 S		√	√	√	√	
6	GMZ			Fragments					√
5	Kunigel V1			Fragments	√	√	√	√	
4	Deponit CAN			Fragments	√	√	√		
3	Asha NW BFL-L	Termoelement + Titanium	3 N		√	√	√		
2	MX80		2 SE		√	√	√	√	
1	MX80		1 N		√	√	√	√	

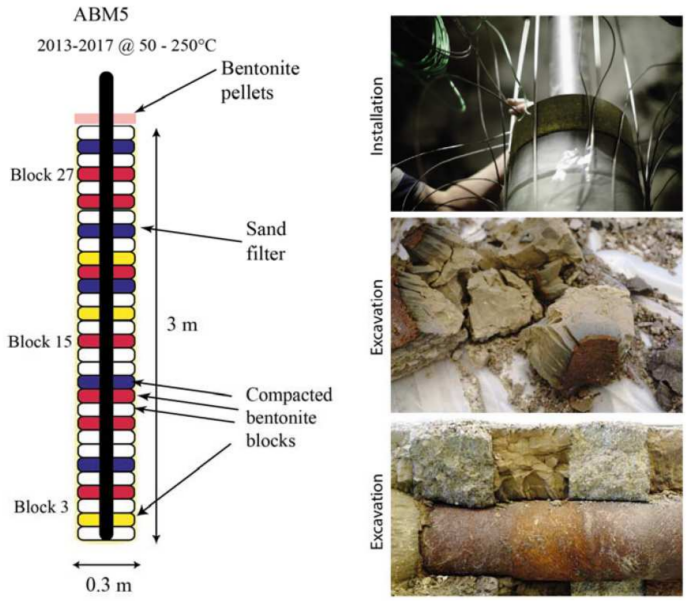

Figure 2. Schematic presentation of the ABM-5 test (**left**) and photographs of a part of the ABM5 experiment before and after dismantling (**right**). The sequence of the different blocks is given in Table 1.

Table 1 lists all samples sent to BGR including information about the state of the sample. Test packages ABM-4–6 are composed of bentonite material only. All bentonites known from previous test packages ABM-1–3 were used again. However, the materials FRI (Friedland clay), COX (Callo-Oxfordian clay), as well as bentonite–quartz mixtures made of MX80 were no longer used in ABM-4–6. Instead, three new bentonite raw materials were used for the first time: GMZ, the Chinese reference material, Asha NW (Ashapura, Mumbai, India), and 'Saponite', a bentonite named after a trioctahedral mineral of the smectite group: saponite. In the present paper, this bentonite is called 'Saponite' to distinguish the raw material from the mineral.

As in the case of previous analyses of ABM-blocks [12,13], each block should be sampled at different distances to the contact. In some cases, only fragments were present, which made it impossible to obtain suitable samples from defined distances. Sampling of the blocks was undertaken at four different distances to the contact (0.1, 1, 5 and 8 cm). A minimum of 2 g was required for a comprehensive characterization. The actual depths at which the 0.1 cm sample was taken, therefore, depended on the available area of the contact. The contact area ranged from 10 to 20 cm^2 and 2 g were collected which, assuming a density of 2 g/cm^3, corresponds to a sampling depth of 0.05–0.1 cm. The contact sample was collected with a sharp knife and the other samples were collected by hand drilling. The samples were then dried at 60 °C for three days and ground using a mortar mill.

The chemical analysis was performed by ACTLABs® using the analytical tools 4B1 QOP Total (Total Digestion using different acids, analysis by ICP-OES), 4C QOP XRF Fusion (Whole Rock Analysis-XRF), and 4F-Cl QOP INAA—Short Lived (INAA). The effect of different water contents on the elemental composition was eliminated by normalizing all values not considering the loss on ignition.

The organic carbon (C_{org}) content was measured by combustion with a LECO CS-444-Analysator after dissolution of the carbonates. Carbonates were removed by treating the samples several times at 80 °C with HCl until no further gas evolution could be observed. Samples of 170–180 mg of the dried material were used to measure the total carbon (C_{total}) content. Total inorganic carbon (C_{inorg}) was calculated by the difference of C_{total} and C_{org}. The samples were heated in the device to 1800–2000 °C in an oxygen atmosphere and the CO_2 and SO_2 were detected by an infrared detector. The device was built by LECO (3000 Lake Avenue, St. Joseph, MI, USA).

Thermoanalytical investigations were performed using a Netzsch 449 F3 Jupiter thermobalance equipped with a DSC/TG sample holder linked to a Netzsch QMS 403 C Aeolus mass spectrometer (MS). Then, powdered material (100 mg) previously equilibrated at 53% relative humidity (RH) was heated from 25 to 1150 °C with a heating rate of 10 K/min. The devices were manufactured by Netzsch (Gebrüder-Netzsch-Straße 19, Selb, Germany).

XRD patterns were recorded using a PANalytical X'Pert PRO MPD Θ–Θ diffractometer (Cu-K_α radiation generated at 40 kV and 40 mA), equipped with a variable divergence slit (20 mm irradiated length), primary and secondary sollers, Scientific X'Celerator detector (active length 0.59°), and a sample changer (sample diameter 28 mm). The samples were investigated from 2° to 85° 2Θ with a step size of 0.0167° 2Θ and a measuring time of 20 s per step. For specimen preparation, the back loading technique was used.

For the detailed clay mineralogical investigation, texture slides of the <2 μm fraction were prepared. Oven-dried clay fractions <2 μm of the contact samples (if available) were dispersed using ultrasound. A suspension containing approximately 60 mg solid clay fraction was sucked through porous ceramic tiles of 27 mm diameter using a vacuum-filter in order to orient the clay minerals (alumosilicates) preferentially parallel to their basal planes. The final solid density was approximately 15 mg/cm^2. These so-called oriented aggregates were x-rayed from 2.5 to 40° 2Θ (air-dried and ethylene glycol solvated) with a step size of 0.03° 2Θ. The measuring time wasa 6 s per step. The scans were run on a PANalytical X'Pert PRO MPD Θ–Θ diffractometer (Co-Kα radiation generated at 40 kV and 40 mA), equipped with a variable divergence slit (20 mm irradiated length), a primary and secondary soller, a proportional counter, and a secondary monochromator.

A Zeiss Sigma 300 V P FEG scanning electron microscope operating at 15 kV was used to evaluate samples on the micro scale using the high-vacuum mode. The microscope was equipped with the following detectors: Bruker Xflash® 6/60 EDX detector, high-definition backscattered electron detector (HDBSD), secondary electron detector (SE2), variable pressure secondary electron detector (VPSE), and an InLens detector for detection of secondary and backscattered electrons, respectively.

For measuring mid (MIR) infrared spectra, the KBr pellet technique (1 mg sample/200 mg KBr) was applied. Spectra were collected on a Thermo Nicolet Nexus FTIR spectrometer (MIR beam splitter: KBr, detector DTGS TEC; FIR beam splitter: solid substrate, detector DTGS PE). The resolution was adjusted to 2 cm^{-1}. Measurements were conducted before and after drying of the pellets at 150 °C in a vacuum oven for 24 h. The spectrometer was built by Nicolet Instruments, Verona Road, Madison, WI, USA.

3. Results and Discussion

All data is summarized in Table S1 (Supplementary Materials).

3.1. Geochemical Profiles

In the LOT experiment, which was also conducted at temperatures higher than 90 °C, a redistribution of sulphate phases (gypsum) was detected [17]. Gypsum was obviously dissolved both near the crystalline host rock and near the heater and precipitated in the center of the blocks. In the ABM1 and ABM2 tests, different S-profiles were measured [12,13], which indicates that locally different conditions (water content and temperature) can lead to different gypsum/anhydrite redistribution profiles. In the LOT experiment, which was setup with MX80 blocks only, this gypsum redistribution was found in many different blocks and at different depths (from 0 to 3 m). Most of the blocks of ABM5 (present study) showed a slight increase of the S content in the central part and some dissolution at the inner and outer parts (Figure 3). This behavior was similar to the results found in the LOT A2 experiment but much less pronounced. The amount of S which precipitated in the central part of the LOT A2 blocks was larger. S concentrations below 0.1 mass% are close to detection limit and hence not discussed further. Most of the samples, however, showed S contents ranging from 0.2 to 0.4 mass%. Three samples showed an untypical behavior. In

block 1 (lowermost sample), a significant increase of the S content directly at the heater was observed. The top block (#30) showed S enrichment at a distance of 1 cm. In both cases, an increase of approximately 0.2 up to 0.5 mass% S was observed. The extraordinary behavior of these two blocks (#1, #30) may result from the special hydraulic properties caused by the fact that there were no other blocks above and below. In the case of block #30, cement pore waters derived from the concrete seal above could have provided different cations and anions (compare [12]). In the case of block 1, however, no concrete was near the block, but the sand base could have promoted water inflow. Blocks 26 and 4, both Deponit CAN, showed the highest initial S content but slightly different profiles. For both samples, slightly lower values were found in the block after the experiment compared to the reference, which confirms that gypsum is at least partly soluble and transported inside the barrier.

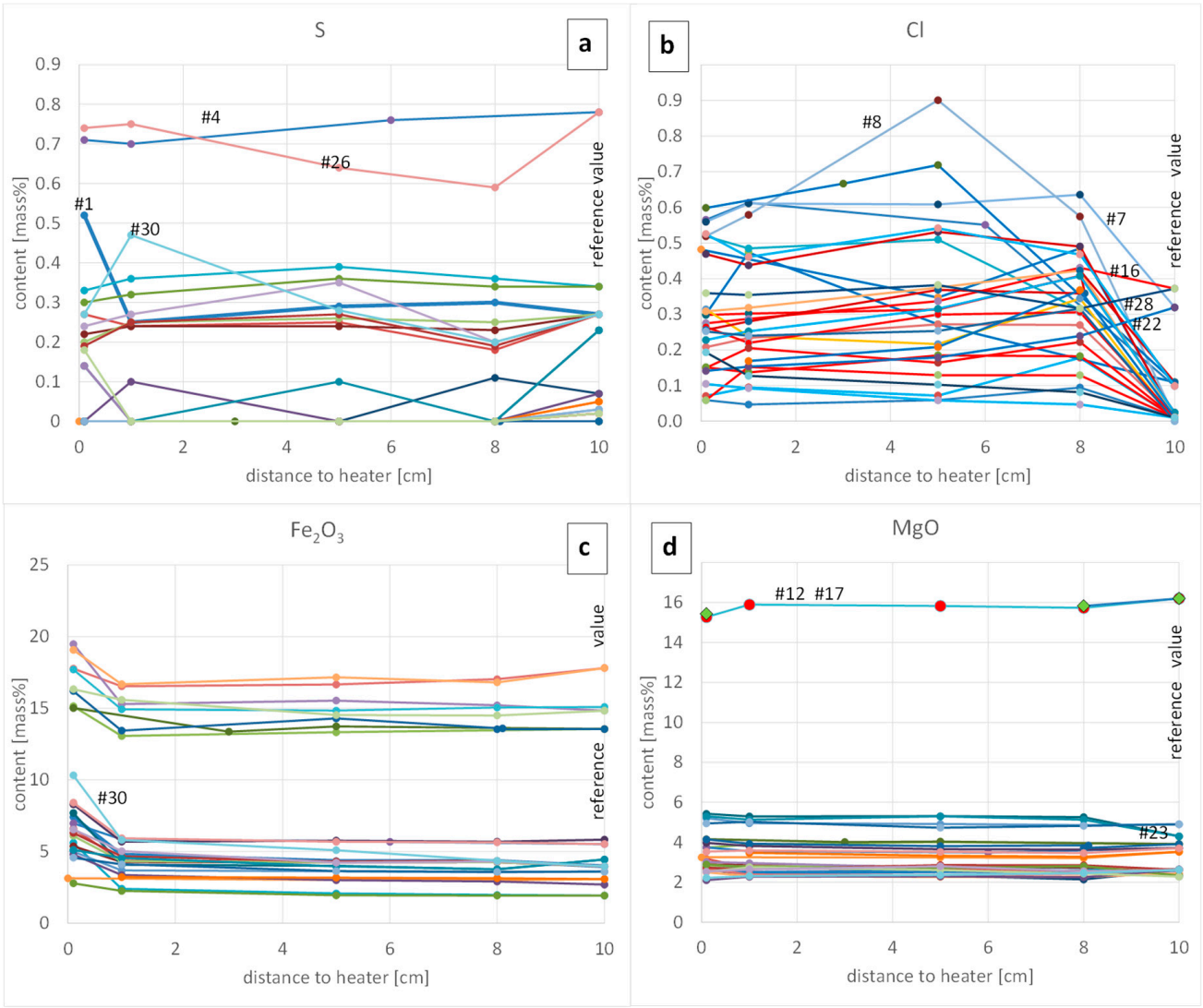

Figure 3. Geochemical profiles of S (**a**), Cl (**b**), Fe_2O_3 (**c**), and MgO (**d**) of all blocks.

Most samples showed an initial Cl content of ≤0.1 mass% and an increase in the reacted blocks which can only be explained by Cl derived from the rock water which migrated into the blocks. In most blocks Cl even reached the heater because the contents measured there were higher compared to the reference materials. The Cl concentrations were not higher in the contact samples of the upper- and lowermost blocks, which suggests that the Cl did not migrate to the heater and then vertically along the bentonite/heater

interface, but was transported parallel to the thermal gradient (horizontally). The Cl concentrations of the ASHA 505 and IKO blocks (#7, #16, #22, #28, Figure 3b) indicate that material properties were less relevant with respect to the resulting Cl profiles than local conditions. Blocks #22 and #28 had a larger initial Cl concentration, and this decreased towards the heater. Blocks #7 and #16, however, showed the opposite effect. IKO showed Cl increase in block #7 and decrease in block #22. Asha 505 showed an increase in block #16 and decrease in block #28. The Cl migration into the blocks apparently did not depend on the material but on local differences which is discussed later.

The Fe contents were interesting because they may reflect canister corrosion. Most of the blocks showed an increase of the Fe_2O_3 content at the contact (0.1 mm sample) of more than 1 mass%. The largest increase was found for the top block (#30: +6.3 mass%). These values can hardly be compared with those of the other studies because of different sampling areas (as explained above). In blocks #20–#30 a slight increase of the Fe_2O_3 content could even be detected in the 1 cm sample. The increase ranged from 0.3 mass% (compared with the reference) up to 2 mass% (#30) and it apparently increased with block number. One may conclude that Fe diffusion into the barrier was more pronounced in the upper blocks, which could result from temperature or water content (discussed later).

Mg enrichment close to the heater was observed in many large-scale tests, regardless of whether Fe or Cu was used. This enrichment is of particular interest because it points towards the neoformation of phases such as trioctahedral smectite and/or brucite (FEBEX experiment) at the expense of dioctahedral smectite, which in turn could result in a reduction of the swelling capacity of the barrier at the heater.

In the ABM2 test [13], MgO enrichments at the contact of 0.0–3.0 mass% were observed. The most significant MgO increase was observed at the face of the FEBEX experiment (+6 mass% MgO [24]) which at least partly can be explained by the fact that a large sampling area was available (about 200 cm^2) and hence the very top could be sampled (<0.1 mm). Using IR spectrometry, the formation of brucite was found, and by XRD, the formation of trioctahedral domains was observed. Fernandez et al. [22] could also observe sepiolite. In the ABM2 experiment, only the formation of trioctahdral phyllosilicate domains was observed (no brucite), commonly associated with a significant MgO increase. In the previous ABM tests and in the present one, the MgO increase, however, was not typical for a special type of bentonite. As an example, the two blocks of Deponit CAN and ROK showed either 0.0–0.3 mass% or 1.8–2.8 mass% MgO increase. These values, therefore, seem to depend more on the local conditions (temperature, water content, type of solution diffusing through the bentonite) than on the type of bentonite. The significantly larger temperature of ABM5 could have affected the formation of Mg-rich phases. Kaufhold et al. [23] showed that the temperature affects the ratio of Mg/Si which can be dissolved from smectites in such a way that it decreases with increasing temperature, which means that the solubility of Si increases more than that of Mg at higher temperature. Accordingly, one could expect Si phases (or Si rich Mg-silicates) to be precipitated at the heater. The data are summarized in Supplementary Table S1 and plotted in Figure 3d. Overall, only a slight increase of the MgO value was observed in the ABM5 test. The largest values (+1 mass% MgO) were observed for the two IBECO Seal bentonites, while all others showed lower values. Notably, a slight decrease or increase of the MgO content compared to the reference value (see Figure 3d) can sometimes be explained by cation exchange (cation exchange data will be discussed in detail in a follow up study). For the first time, a trioctahedral smectite (saponite) was tested in a deposition test (in the 'Saponite' blocks). Interestingly, a slight decrease of the MgO content at the heater was observed for both 'Saponite' samples. The curve of #12, however, is not complete because it could only be sampled at the contact. The three points shown in Figure 3d, however, are identical to those measured for block #17 which was also made out of 'Saponite'. Both 'Saponite' blocks, therefore, show an MgO decrease at the heater which can be explained by cation exchange and Fe increase. Sample #17 contained 36 meq/100 g exchangeable Mg before and only 4 meq/100 g after the test which explains part of the MgO decrease. The missing MgO decrease can be explained by the increase of

Fe_2O_3 caused by corrosion which adds to the contact sample hence relatively decreasing the other elements.

For blocks #11 and #23 (both IBECO) more MgO was found in the entire blocks compared to the reference material. This neither can be explained by the small amount of carbonate dissolution nor based on cation exchange. The reason for this difference cannot be explained yet.

3.2. X-ray Diffraction

In bulk XRD, almost all samples showed a shift of the d_{001} peak position which can be explained by cation exchange due to its impact on the bentonite water content after drying in typical laboratory conditions. Differences other than d_{001} shifting such as varying muscovite/feldspar/quartz peak intensities were also observed, but these do not necessarily point towards actual mineral reactions. Differences of these intensities can also be explained by preferred orientation. Moreover, the reference samples were recorded with slightly higher intensity which translates into a better signal/noise ratio. Generally, XRD is not a method to unambiguously detect minor mineral changes. Varying peak intensities may point to actual mineral reactions, but these should be validated based on chemical data. All observed changes detected by XRD are summarized in Figure 4.

Most of the mineralogical changes observed were related to the dissolution/precipitation of C- and S-phases. As an example, gypsum was dissolved in MX80 blocks #8, #15, and #20 whereas gypsum remained stable in the bottom and top blocks made of the same material. Calcite was dissolved in both Ibeco Seal (IBE) blocks #11 and #23 (partly). Dolomite intensities were lower in both Calcigel blocks (#10, #26), indicating partial dissolution. Results of previous large-scale tests showed that the (partly) soluble phases can be dissolved anywhere in the barrier and precipitated elsewhere. In the ABM1 test [12], the dissolution of cristobalite and clinoptilolite was observed. In the ABM5 test, cristobalite intensities were lower only in the Deponit CAN blocks (#4, #26), possibly indicating dissolution. No cristobalite or clinoptilolite dissolution was observed in the other blocks of GMZ, Febex, and MX80. In laboratory experiments with NaOH solutions Karnland et al. [25] reported evidence for cristobalite dissolution in Wyoming bentonite samples. However, pH conditions were obviously lower in ABM5 as the observed dissolution was much lower. The identification of traces of siderite is particularly challenging because of peak coincidences with apatite and partly muscovite. Apatite was observed in Asha NW and ROK. The unambiguous identification of siderite, therefore, is not possible in these samples and other methods such as simultaneous thermal gas (STA) have to be used. No evidence for anhydrite precipitation was observed in ABM5, in contrast to ABM2.

Special attention was paid towards changes of the d_{060} reflexes which in previous tests indicated the presence of trioctahedral phases at the heater or in outer parts of the blocks. All but one material consist of dioctahedral smectite. Such trioctahedral phases were found at the contact to the heater before [11–13,24] based on XRD and IR, supported by an increase in MgO concentration (XRF). In the ABM5 samples, nearly no such changes of the d_{060} XRD intensities were observed, although some MgO enrichment was observed. The extent of the MgO enrichment at the heater, however, was small comparted with yet published results. The largest MgO increase was found in both Ibeco Seal blocks (#11: +1.1 mass% MgO, #23: +1.0 mass% MgO). Moreover, some MgO enrichment was found in block #16 (0.7 mass%) and block #21 (0.6 mass%). However, no changes of the d_{060} reflection were found for any of these blocks with MgO increase (Figure 5b). The 'Saponite' samples (#12, #17) on the other hand showed some decrease of the MgO content at the heater. This bentonite raw material contains trioctahedral smectite (saponite). However, no changes of the d_{060} reflection could be observed either (Figure 5d). An indication for the presence of trioctahedral phases was found in a #7 (Ikosorb) (Figure 5c) and #27 (Calcigel), not shown. In contrast to former ABM experiments, such trioctahedral phases are indicated not only at the contact to the heater, but also in outer parts of the blocks (marked by arrows in Figure 5c).

distances from heater (cm)					sulphate phases									
		d(060)			gypsum					pyrite XRD				
Block	Material/abbreviation	REF	0.1	new (0-1)	REF	0.1	1	5	8	REF	0.1	1	5	8
30	MX80	1.498	✓		+	(?)	+	+		+				?
29	MX80	1.498	✓		+	+	(?)			+	(?)	?	(?)	?
28	Asha 505	1.500	✓		(?)	(?)				(?)	(?)	(?)		
27	Calcigel (CAL)	1.498	no contact sample			X	X	X			X	X	X	
26	Dep. CAN	1.498	✓		+	+	+	?	(?)	+	(?)	(?)	(?)	(?)
25	Febex	1.499	✓											
24	GMZ	1.498(5)	no contact sample			X					X			
23	Ibeco Seal (IBE)	1.498	✓											
22	Ikosorb (IKO)	1.495	✓											
21	Kunigel V1 (JNB)	1.498	✓							+	?	?	?	?
20	MX80	1.498	✓		+					+	?	(?)	(?)	?
19	Asha-NW BFL-L	1.500	✓											
18	Rokle (Rawra)	1.505	✓											
17	Saponite	1.512	✓											
16	Asha 505	1.500	✓		(?)	(?)								
15	MX80	1.498	✓		+					+	(?)	(?)	(?)	(?)
14	Rokle (Rawra)	1.505	✓											
13	Febex	1.499	✓											
12	Saponite	1.512	✓				X	X				X	X	
11	Ibeco Seal (IBE)	1.498	✓											
10	Calcigel (CAL)	1.498	✓											
9	Asha-NW BFL-L	1.500	✓				X		X			X		X
8	MX80	1.498	✓		+					+	(?)	(?)	(?)	(?)
7	Ikosorb (IKO)	1.495	✓	1.54(5)										
6	GMZ	1.498(5)	no contact sample			X	X	X	X		X	X	X	X
5	Kunigel V1 (JNB)	1.498	✓							+	?	?	?	?
4	Dep. CAN	1.498	✓		+	+	(?)	(?)	X	+	(?)	(?)	(?)	X
3	Asha-NW BFL-L	1.500	✓						X					X
2	MX80	1.498	✓		+	(?)	(?)	(?)		+	(?)	(?)	(?)	(?)
1	MX80	1.498	✓		+	+	?	+	+	+	?	?	?	?

	inorganic carbon phases														
	calcite					dolomite/ankerite					siderite				
Block	REF	0.1	1	5	8	REF	0.1	1	5	8	REF	0.1	1	5	8
30															
29															
28	(?)	+	+	+	+										
27	+	X	X	X		++	X	X	X	+		X	X	X	
26	++	+	++	++	++	+	+	+	+	+	(?)	(?)	(?)	(?)	
25	+	+	+	+	+										
24		X					X					X			
23	+	+	(?)		?	+									
22	+	+	+	+	+										
21	+	+	+	+	+						(?)	(?)	(?)	(?)	
20															
19	++	+	+	+	+						+	?	+	+	+
18	?														
17	+	+	+	+	+	+		?	+	?					
16	(?)	+	+	+											
15															
14	?														
13	+	+	+	+	+										
12	+	+	X	X	+	+	(?)	X	X	+			X	X	
11	+	(?)				+									
10	+	(?)	(?)	(?)	(?)	++	+	+	+	+	(?)	+	+	+	+
9	++	+	X	+	X			X		X	+	+	X	+	X
8															
7	+	+	+	+	+										
6		X	X	X	X		X	X	X	X		X	X	X	X
5	+	+	+	+	+						(?)	(?)	(?)	(?)	
4	++	++	++	++	X	+	+	+	+	X	(?)	(?)	(?)	(?)	X
3	++	+	+	+	X					X	+	(?)	(?)	(?)	X
2															
1															

	cristobalite					goethite					clinoptilolite				
Block	REF	0.1	1	5	8	REF	0.1	1	5	8	REF	0.1	1	5	8
30	+	+	+	+	+										
29	+	+	+	+	+										
28						+	+	+	+	+					
27		X	X	X			X	X	X			X	X	X	
26	+	(?)	(?)	(?)	(?)										
25	+	+	+	+	+										
24	+	X		++	++		X					X			
23															
22	+	++	++	++	++										
21											+	+	+	+	+
20	+	+	+	+	+										
19															
18						?	?	?	?	?					
17															
16						+	+	+	+	+					
15	+	+	+	+	+										
14						?	?	?	?	?					
13	+	+	+	+	+										
12			X	X				X	X				X	X	
11															
10															
9			X		X			X		X			X		X
8	+	+	+	+	+										
7	+	++	++	++	++										
6	+	X	X	X	X		X	X	X	X		X	X	X	X
5											+	+	+	+	+
4	+	(?)	(?)	(?)	X					X					X
3					X					X					X
2	+	+	+	++	+										
1	+	+	+	+	+										

Figure 4. Summary of mineralogical changes detected by XRD powder diffraction (X = samples not available, "+" = clearly identified, "(?)" = could be present, difficult to decide) and additional techniques for trace phases (carbonate group minerals, sulphates, pyrite). MX80 samples are marked yellow.

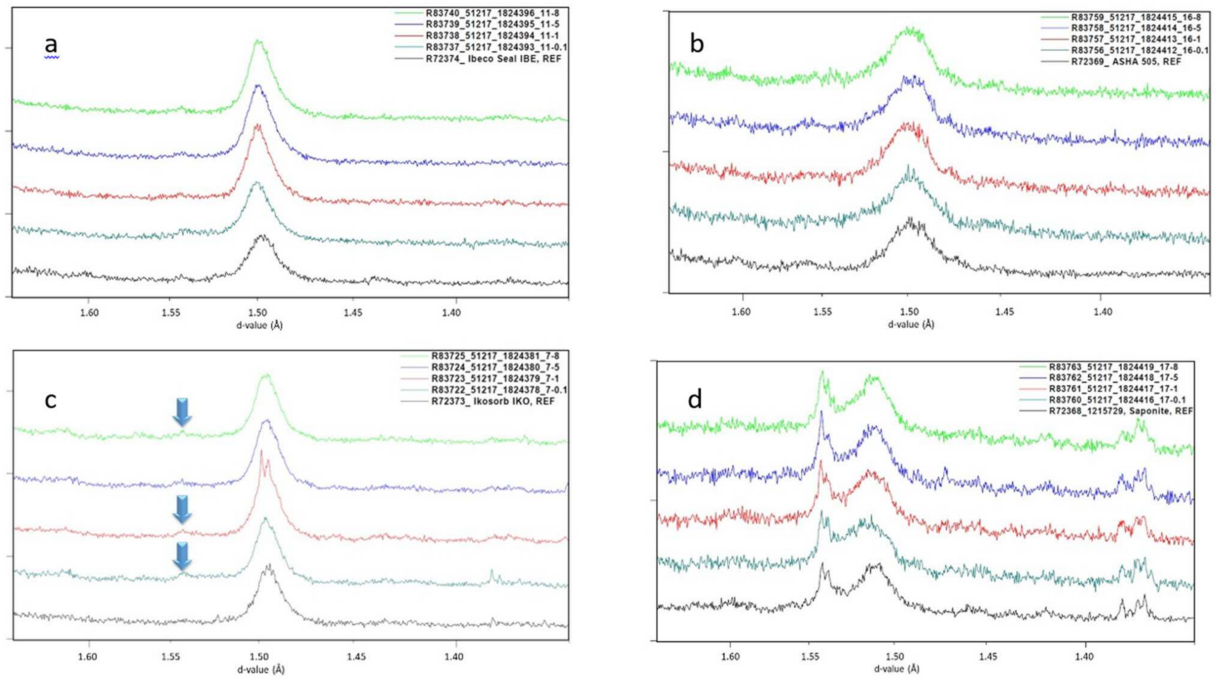

Figure 5. XRD analysis of the d_{060} region of dioctahedral smectites in (**a**) #11 (Ibeco Seal), (**b**) #16 (Asha 505), both showing no evidence for presence of trioctahedral phases; whereas presence of trioctahedral phases could be indicated in (**c**) #7 (Ikosorb). In the only block with trioctahedral smectites (**d**) #17 ('Saponite') no evidence for presence of (additional) dioctahedral phases was observed.

XRD analyses of clay fractions of all bentonites from the samples at the contact to the heater (0.1 cm) or of fragments—if such samples were not available—were performed to verify if smectites became interstratified during the ABM5 test. Results indicated no additional interstratification of smectites for any block in comparison with the reference materials ('Saponite' and GMZ data are shown as an example in Figures 4 and 6a,b). Dioctahedral smectites of GMZ (Figure 6b) remained fully expandable (i.e., no illitization) and all bentonites showed the same behavior. The saponite clay minerals in bentonite 'Saponite' initially shows a broad peak at ca. 10.5 Å, which remained unchanged after the experiment (Figure 6a). This intensity can be explained as smectite with collapsed/non expandable layers. 'Saponite' also contains traces of chlorite, serpentine, and talc.

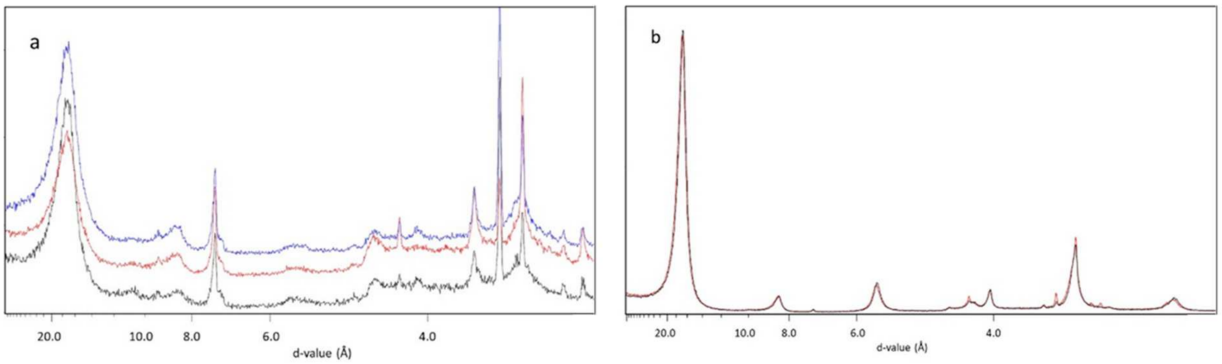

Figure 6. XRD peak positions for clay fractions of (**a**) 'Saponite' from the contact to the heater (0.1 cm) of blocks #12 (red) and #17 (blue, upper scan) and of (**b**) GMZ block #6 (fragments with unknown distance to the heater) and the of the according REF samples (both in black) after EG solvation.

3.3. Simultaneous Thermal Analysis (STA) and Elemental C-/S-Analysis

STA was performed to investigate the C- and S-phase changes at the interface. As discussed before, carbonates and sulphates can be dissolved precipitating elsewhere and pyrite can be oxidized. The STA detection limit of theses phases is low because of the sensitive mass spectrometer (MS). Pyrite, which is detected by a peak of the MS-SO_3 curve between 450 and 500 °C, was found in the bentonites used for blocks #4 and #5 as an example (Figure 7). Interestingly, the pyrite at the contact of block #4 was preserved (could still be detected in the sample taken after the test) but it was oxidized at the contact of block #5. Both blocks were close together, but the different results indicate that the redox potential and/or hydraulic conditions differed inside the blocks. In some samples (#4, #5, #10 in Figure 7), a decrease of the carbonate peak and an increase of the siderite peak (between 500–600 °C) was found.

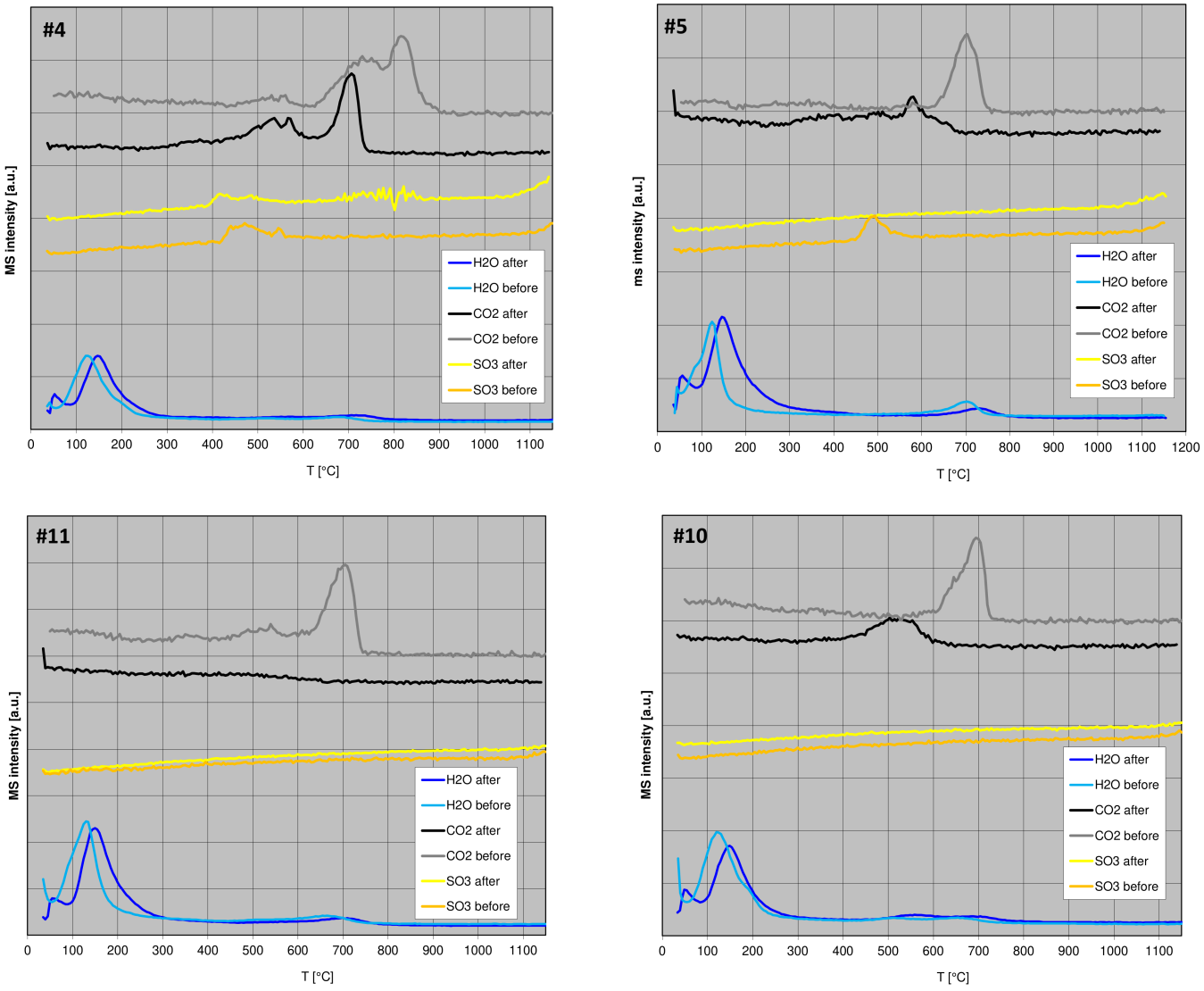

Figure 7. STA-MS curves (H_2O, CO_2, SO_3) of four selected blocks ("before" = reference; "after" = contact sample).

Carbonate dissolution and precipitation was found in different medium to large scale deposition tests. Elemental combustion analysis of all samples indicates that different carbonate redistribution reactions occurred. Most samples had a C_{inorg} content of <0.2 mass% and did not show any carbonate redistribution. However, some specific reactions could be identified: A few samples showed some carbonate enrichment in the center of the blocks

with larger values compared to the reference (e.g., #1, #14). This indicates that carbonate was either transported into the barrier by the saturating fluid or that carbonate was dissolved in other blocks and transported vertically. Significant carbonate dissolution was observed for both blocks made out of Ibeco Seal (#11, #23; Figure 8). Only the carbonates of the contact sample of #23 seemed to be preserved. Similarly, the blocks made out of Asha NW (#9, #19) showed much lower C values in the blocks compared with the reference which points towards carbonate dissolution. Only the sample taken 1 cm from to the heater showed the same values as the precursor. The largest carbonate content was found in the sample Deponit CAN (about 0.9 mass% C_{inorg}). Both blocks were not in the hottest part but showed different reactions. In block #26 carbonate was dissolved near the heater whereas it precipitated near the heater in block #4.

The content of inorganic and organic carbon was determined by combustion (LECO) with and without acid sample pre-treatment. An increase of the C content in the acid treated material would be interpreted as increased organic C because siderite does not fully dissolve in the acid. In the ABM1 and ABM2 tests molykote® was used as lubricant which provided an additional source of organic C and hence complicated the interpretation of elemental C data. The ABM5 was setup without lubricant (it was used during the compaction of the blocks but was removed from the blocks prior to the experiment, by physically removing the outermost 2–3 mm of bentonite from the blocks inner surface by abrasion), which allowed to reveal the formation of siderite at the contact. Some samples showed a decrease of the calcite STA peak (700–800 °C) and an increase of the STA peak between 500 and 600 °C. By elemental C analysis, an increase of the C_{org} content was found for these samples. Both methods hence indicate the formation of siderite at the contact. This reaction, however, was not observed in all blocks. In some, no changes of the carbonates were observed, and in others, dissolution was observed without the precipitation of siderite (e.g., #11). Calcigel showed strong lowering of XRD intensities of dolomite as well as calcite (less clear), along with the formation of siderite (#10, #27).

Siderite formation was observed before. According to Martin et al. [26], Romaine et al. [27], and Mendili et al. [28], magnetite is coating the iron surface and siderite forms on top of the magnetite. They used COX clay which contains carbonates. Moreover, Savoye et al. [29] found siderite formation if carbonate is present, which, however, is not the case in all bentonites. Saheb et al. [30] found Fe-hydroxo-carbonate as corrosion product, which indicates that different Fe-carbonate phases can be present.

The most significant changes detected by XRF, STA, and elemental C are summarized in Table 2. Notably, IR-spectrometry was also used—as in ABM2—but no specific changes except for carbonate dissolution/precipitation could be found. In ABM2, a band at 3740 cm^{-1} pointed towards the formation of free silica. This band could not be observed in any of the ABM5 contact samples.

Table 2. Summary of measured differences of the contact sample (0.1 cm) of each block compared with the reference material. Negative values indicate dissolution and positive values correspond to increased concentrations. No contact samples were available of #6, #24, and #27. Bold numbers represent most significant changes, "-" = decrease, "?" = change possible but not unambiguous, "(ox.)" = oxidation (present as sulphate afterwards), "diss" = dissolution.

		XRF	XRF	STA	STA	STA	C/S Analyzer		
		ΔMgO	**ΔFe_2O_3**	**CaMgCarb**	**Siderite**	**Pyrite**	**ΔC_{org}**	**ΔC_{inorg}**	**S**
30	MX80	−0.4	**6.3**			-, ?	**0.3**	−0.1	0.0
29	MX80	−0.1	2.6			-, ?	0.0	0.0	0.0
28	Asha 505	0.2	1.5				0.1	0.0	**0.2**
27	Calcigel								
26	Deponit CAN	−0.2	2.9	-	+	-, (ox.)	0.1	**−0.3**	0.0
25	Febex	0.0	1.0				0.0	−0.1	0.0
24	GMZ								

Table 2. *Cont.*

		XRF	XRF	STA	STA	STA	C/S Analyzer		
		ΔMgO	**ΔFe_2O_3**	**CaMgCarb**	**Siderite**	**Pyrite**	**ΔC_{org}**	**ΔC_{inorg}**	**S**
23	Ibeco SEAL	1.0	0.7	-			−0.1	−0.1	**−0.2**
22	Ikosorb	−0.5	2.1				0.1	−0.2	−0.1
21	Kunigel V1	0.6	0.9		+, ?	-, (ox.)	0.1	0.0	0.0
20	MX80	0.1	2.3				0.0	0.0	−0.1
19	Asha NW BFL-L	0.2	2.7	-	+		0.1	**−0.4**	0.0
18	Rokle	0.1	1.3				0.0	−0.1	0.0
17	Saponite	−0.9	2.6	-			−0.1	−0.1	0.0
16	Asha 505	0.7	**4.6**				0.1	0.1	0.1
15	MX80	0.2	2.1			-, ?	0.0	0.0	−0.1
14	Rokle	0.2	0.0				0.0	0.0	0.0
13	Febex	0.3	1.4				0.1	−0.1	0.0
12	Saponite	−0.8	2.4	-	+		0.1	−0.2	0.0
11	Ibeco SEAL	1.1	3.2	-			0.0	**−0.6**	**−0.2**
10	Calcigel	0.3	2.5	-	+		**0.2**	−0.2	0.0
9	Asha NW BFL-L	0.2	1.5	-	+		0.1	**−0.3**	0.0
8	MX80	0.3	1.4				0.0	0.0	−0.1
7	Ikosorb	0.0	1.7				0.0	−0.1	0.1
6	GMZ								
5	Kunigel V1	0.4	3.7	-	+	-, (ox.)	0.1	0.0	0.0
4	Deponit CAN	0.0	1.4	-	+	no ox.	**0.4**	0.0	−0.1
3	Asha NW BFL-L	−0.2	1.6	-, (diss)			0.1	**−0.5**	0.0
2	MX80	0.6	2.6			-, ?	0.1	0.0	0.0
1	MX80	0.2	3.4			-, ?	0.0	0.0	**0.3**

3.4. SEM

Some blocks which showed the most significant changes (see Table 2) were investigated by scanning electron microscopy (SEM), focusing on the interface.

The lowermost block #1 showed the highest increase of S and appreciable increase of iron. The surface was dark green with some approximately 1 mm^2 large black spots. Separated particles of the black spots were ferromagnetic, pointing to the presence of magnetite, which is a common corrosion product near the Fe heater. EDX mapping proved the accumulation of Fe at the contact as well as gypsum precipitations (Figure 8a,b).

Block #4 showed a moderate Fe increase. Accordingly, no significant differences were found when mapping the edge of the surface and the bentonite block (Figure 8c). The surface of block #4 showed the largest increase of organic material (LECO), which according to STA could at least partly be explained by siderite. By SEM, however, no newly formed carbonates were found, only a few gypsum crystals at the contact. Instead, a few hyphae were found, which are supposed to result from organic contamination.

The contact of block #10 also showed a significant increase of organic carbon, which based on STA could unambiguously be explained by siderite formation. On the surface, however, traces of microbiological activity were found consisting of hyphae pointing towards the presence of fungi. The concentration is too low to explain the increase of elemental organic-C and the fungi are not believed to have persisted throughout the heat treatment. They most probably formed during storage, although their metabolism could not be characterized further. This has to be systematically investigated in future. The Fe_2O_3 increase at the contact was moderate (+2.5 mass%), but SEM-EDX mapping revealed an undulating seem (50–300 μm) in which Fe was enriched.

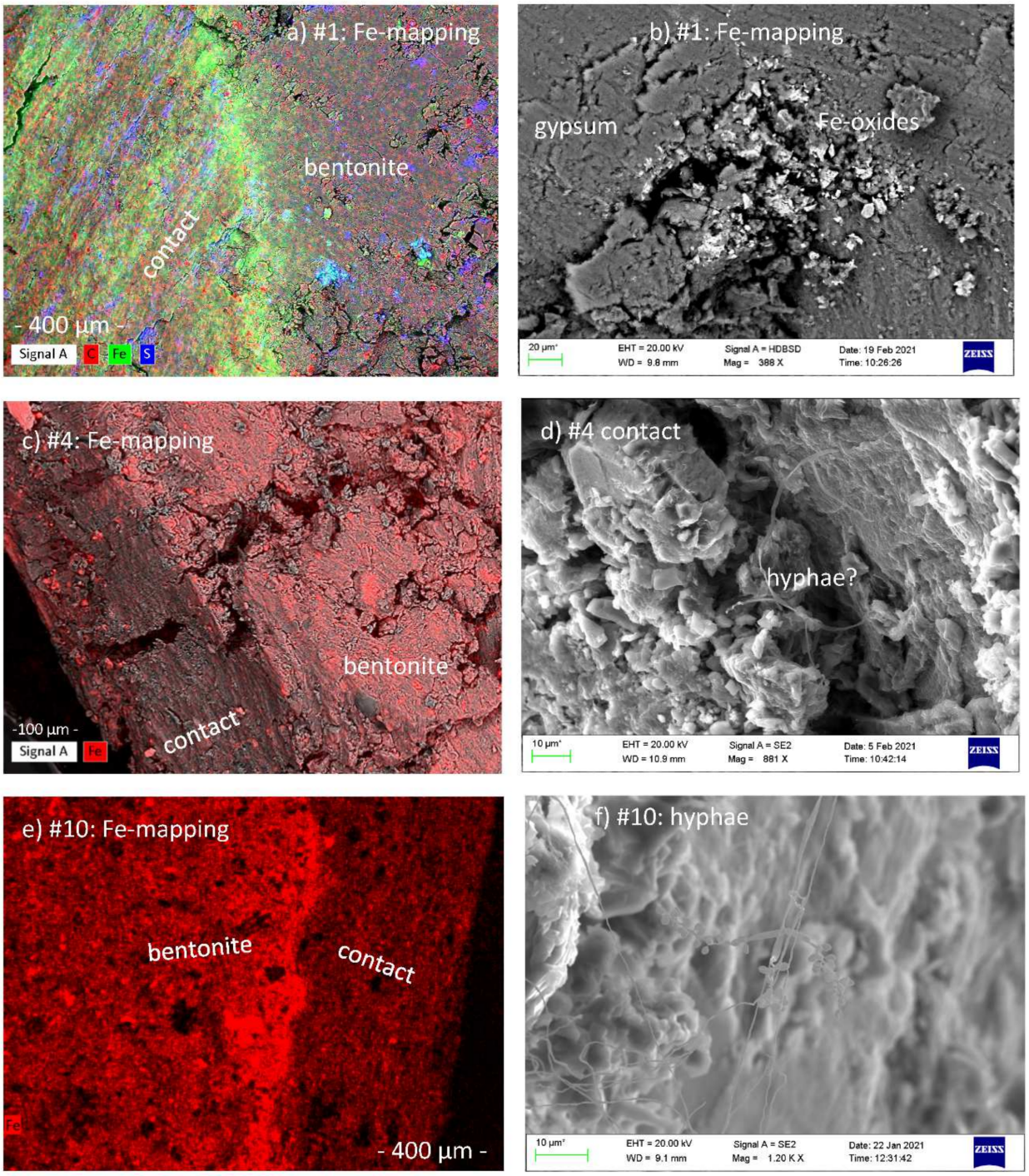

Figure 8. SEM images of the surface of selected samples. (**a**,**b**) block 1; (**c**,**d**) block 4; (**e**,**f**) block 10.

Block #16 also showed a significant Fe increase. Figure 9a,b show views on the surface. EDX mapping proved the presence of a homogenous Fe coating (green) with some gypsum spots on top of it.

In block #30 the most significant increase of Fe was found (+6.3 mass%). On the surface, massive Fe coatings were found, which proved to be ferromagnetic. By SEM, however, no small cubic crystals typical of magnetite, but rather a network of fine needles about 500 nm in length was found. Other areas of the surface were coated by gypsum needles (Figure 9e) and isometric gypsum particles (Figure 9f).

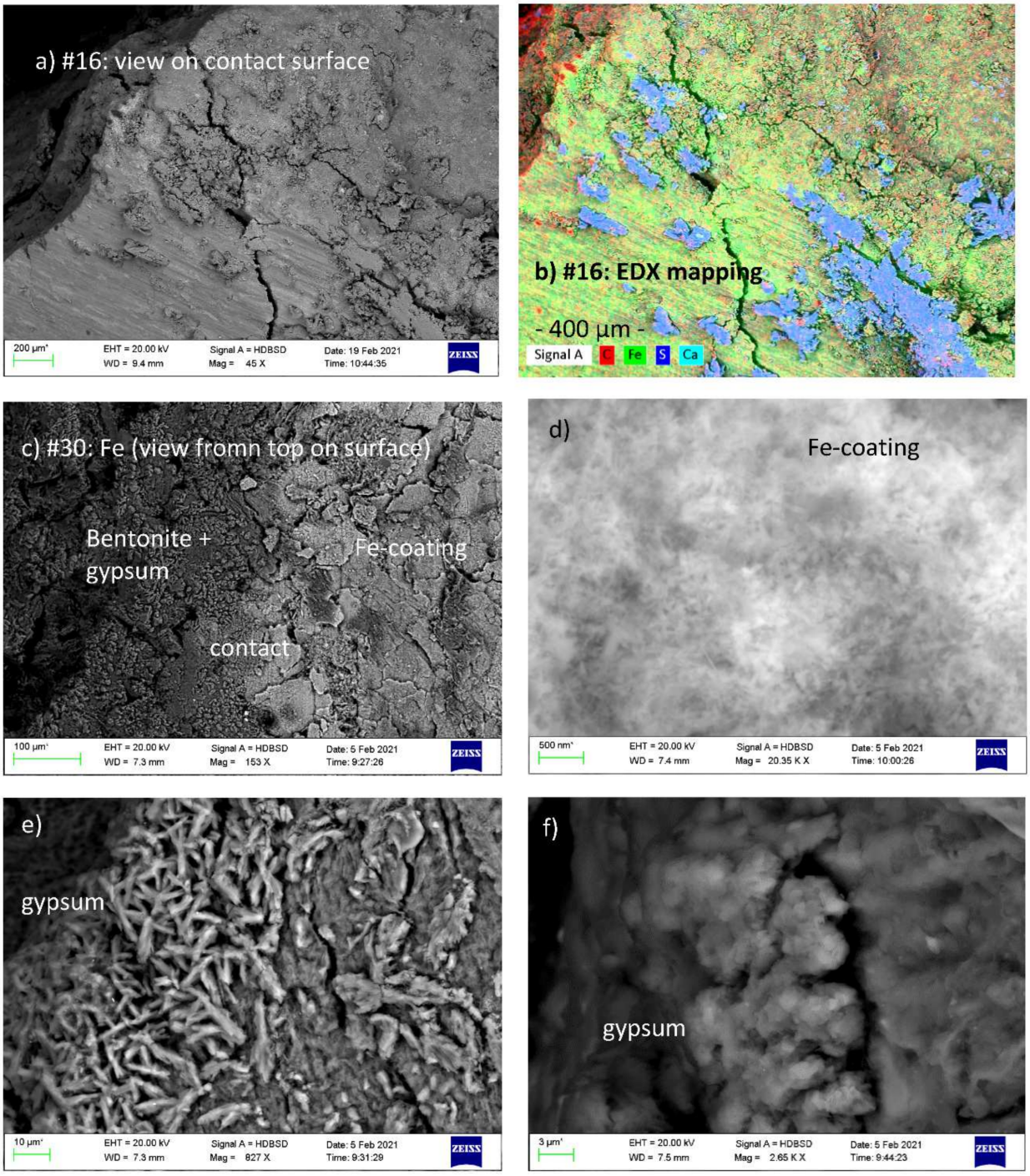

Figure 9. SEM images of the surface of selected samples. (**a**,**b**) block #16, (**c**–**f**) block #30.

3.5. Effect of Temperature

Within an up- or large-scale experiment, locally different conditions may exist, which could lead to different reactions. In the case of the ABM tests, the different materials may have an additional effect on the heterogeneity. The temperature profile (Figure 10) depends on the location and power of the heater and on the thermal conductivity of the adjacent bentonite. The water content (Figure 10) depends on the water uptake of the clays, but also on the drainage system. The bentonite blocks were supposed to be water saturated before heating to the maximum temperature. In the ABM5-test, sand was around the bentonite blocks in which the water could evenly distribute outside the barrier. The hydraulic

conditions probably changed with increasing the temperature because of the relatively lower pressure in the sand filter. Moreover, no effect of the fracture in the deposition hole at a depth of about 0.8 m on the water saturation was found. The water content was higher at the bottom probably because the water gathered at the bottom of the deposition hole. The water content and the resulting degree of saturation were therefore larger in the lower 30% of the test, which also affected the dry density (which was lower in the lowermost part). In order to investigate if these locally different conditions could have affected the results, selected chemical differences were plotted depending on depths (Figure 10). No relation of MgO with burial depths could be identified (not shown). The same holds true for inorganic and organic C and total S. The Cl content was on average higher in the lowermost 30% (blocks #1–#10) of the package, which can be explained by the higher water content (and degree of saturation). Most of the Cl is assumed to result from the external saturating fluid. No relation was found between the Fe increase at the contact and the depths. Only block #30 showed a much larger Fe increase, which, however, may have resulted from the special conditions at the top (more oxygen, concrete fluids), but this could not be proven. Interestingly, the Fe increase in 1 cm distance from the heater was more pronounced in the upper blocks, which cannot be explained yet.

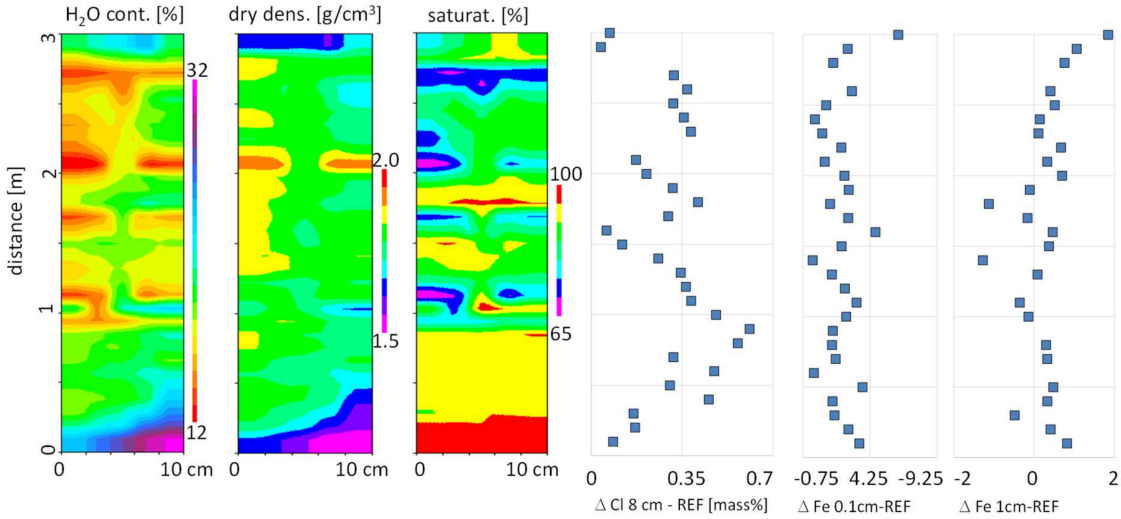

Figure 10. Water content, dry density, and degree of saturation measured before termination of the ABM5-test compared with the changes of the Cl- (8 cm distance to the heater) and Fe-content (at 0.1 and 1 cm distance from the heater). Additional information about the T-profile is provided in Figure 1.

4. Summary and Conclusions

Results of XRD, XRF, elemental C and S, and STA were not always concise, which results from the fact that many mineralogical changes were close to the detection limit of the methods. Some unambiguous results, however, were found.

Cl concentrations did not depend on material properties or temperature. The Cl content was assumed to result from effects such as inflowing water. On average, a higher Cl increase was found in the lower part of the test, but at the very bottom, the highest water content and lowest Cl increase were found. The reason for different Cl increases could, therefore, not be identified and are supposed to be related to the hydraulic conditions outside and inside the blocks. An additional effect of temperature cannot be excluded.

In blocks #1–#19, the Fe_2O_3 increase was restricted to the contact. Blocks #20–#30 all showed a slight to significant increase of the Fe content, even in the 1 cm sample, which indicated both increased corrosion and migration of Fe into the blocks in the upper parts of the test, which can hardly be explained because of the lower water content and hence lower degree of saturation in this zone.

Mg enrichment at the heater, as observed in most of the previous bentonite field experiments, was comparably low. Interestingly the Mg rich 'Saponite' even lost some of its Mg content, also indicating some mobility of Mg within these compacted clays.

Carbonate dissolution and precipitation (redistribution) showed different patterns, which does not allow to derive a general rule. Different profiles were observed for the same material and temperature. Therefore, the differences of the profiles cannot be explained by either material properties (type of carbonate present) or by the different temperatures. Carbonate redistribution is likely more affected by local differences, possibly of porosity and water content. Because of the absence of any lubricant, it was possible to observe a recrystallization of carbonate in some contact samples, where siderite formed at the expense of Ca(Mg)carbonates (proved by STA and LECO and sometimes XRD).

The gypsum redistribution resembled that which was found in the LOT test (increase in the center of the blocks), but this effect was much less pronounced in the ABM5 test. The most significant gypsum increase was found in the upper and lowermost blocks. The identified gypsum may possibly have been anhydrite in the experiment that may have hydrated during storage, as there are indications of moisture in the samples during the storage.

By XRD, no additional interstratification of smectites for any block in comparison with the reference materials was indicated. The neoformation of trioctahedral phases could be indicated only in block #7 (Ikosorb). In the only block with trioctahedral smectites as starting material, #17 ('Saponite'), no evidence for the presence of (additional) dioctahedral phases was observed.

Supplementary Materials: The following are available online at https://www.mdpi.com/article/10.3390/min11070669/s1. Table S1: Compilation of geochemical data of all samples taken from the blocks.

Author Contributions: STA- and chemical analysis, S.K.; interpretation, S.K. and P.S.; writing, S.K., R.D., K.U., D.S., and P.S.; CEC- and XRD-analysis, R.D. and K.U.; rietveld refinement, K.U.; conduction of test and sampling, D.S.; managing test and sampling, P.S. All authors have read and agreed to the published version of the manuscript.

Funding: The work was funded by the EURAD project (work package "HiTec").

Data Availability Statement: Not applicable.

Acknowledgments: The authors are grateful to Niko Götze, Frank Korte, Natascha Schleuning, Melanie Hein, and Andre Marx for their great analytical work.

Conflicts of Interest: The authors declare no conflict of interest.

References

1. Dohrmann, R.; Kaufhold, S.; Lundqvist, B. The role of clays for safe storage of nuclear waste. In *Handbook of Clay Science, Techniques and Applications*; Bergaya, F., Lagaly, G., Eds.; Elsevier: Amsterdam, The Netherlands, 2013; Volume 5B, pp. 677–710. ISSN 1572-4352.
2. Sellin, P.; Leupin, O. The use of clay as an engineered barrier in radioactive waste management—A review. *Clays Clay Miner.* **2014**, *61*, 477–498. [CrossRef]
3. Kaufhold, S. (Ed.) Bentonites—From mine to application. In *Geologisches Jahrbuch B 107*; Schweizerbart: Stuttgart, Germany, 2020; ISBN 978-3-510-96859-6.
4. Eisenhour, D.D.; Brown, R.K. Bentonite and its impact on modern life. *Elements* **2009**, *5*, 83–88. [CrossRef]
5. Kaufhold, S.; Dohrmann, R. Distinguishing between more and less suitable bentonites for storage of high-level radioactive waste. *Clay Miner.* **2016**, *51*, 289–302. [CrossRef]
6. Eng, A.; Nilsson, U.; Svensson, D.; Äspö Hard Rock Laboratory. *Alternative Buffer Material*; Installation Report SKB IPR-07-15; Svensk Kärnbränslehantering AB: Stockholm, Sweden, 2007. Available online: http://www.skb.com/publication/1633130/ipr-07-15.pdf (accessed on 1 June 2021).
7. Muurinen, A. *Studies on the Chemical Conditions and Microstructure in Package 1 of Alternative Buffer Materials Project (ABM) in Äspö*; Posiva WR 2010–11; Posiva Oy: Olkiluoto, Finland, 2010.

8. Kumpulainen, S.; Kiviranta, L. *Mineralogical, Chemical and Physical Study of Potential Buffer and Backfill Materials from ABM Test Package 1*; Posiva WR 2011–41; Posiva Oy: Olkiluoto, Finland, 2011. Available online: https://inis.iaea.org/collection/NCLCollectionStore/_Public/43/068/43068661.pdf (accessed on 1 June 2021).
9. Svensson, D.; Dueck, A.; Nilsson, U.; Sandén, T.; Lydmark, S.; Jägerwall, S.; Pedersen, K.; Hansen, S. *Alternative Buffer Material. Status of Ongoing Laboratory Investigation of Reference Material and Test Package 1. SKB TR-11-06*; Svensk Kärnbränslehantering AB: Stockholm, Sweden, 2011.
10. Svensson, P.D.; Hansen, S. Redox chemistry in two iron-bentonite field experiments at Äspö hard rock laboratory, Sweden: An XRD and Fe K-edge XANES study. *Clays Clay Miner.* **2013**, *61*, 566–579. [CrossRef]
11. Svensson, P.D. The Bentonite Barrier. Swelling Properties, Redox Chemistry and Mineral Evolution. Ph.D. Thesis, Faculty of Engineering, Lund University, Lund, Sweden, 2015. Available online: https://portal.research.lu.se/ws/files/5584182/5045914.pdf (accessed on 1 June 2021).
12. Kaufhold, S.; Dohrmann, R.; Sandén, T.; Sellin, P.; Svensson, D. Mineralogical investigations of the alternative buffer material test—I. Alteration of bentonites. *Clay Miner.* **2013**, *48*, 199–213. [CrossRef]
13. Kaufhold, S.; Dohrmann, R.; Götze, N.; Svensson, D. Characterisation of the second parcel of the alternative buffer material (ABM) experiment—I mineralogical reactions. *Clays Clay Miner.* **2017**, *65*, 27–41. [CrossRef]
14. Kumpulainen, S.; Kiviranta, L.; Korkeakoski, P. Long-term effects of an iron heater and Äspö groundwater on smectite clays: Chemical and hydromechanical results from the in situ alternative buffer material (ABM) test package 2. *Clay Miner.* **2016**, *51*, 129–144. [CrossRef]
15. Dohrmann, R.; Kaufhold, S. Characterisation of the second package of the alternative buffer material (ABM) experiment—II Exchangeable cation population rearrangement. *Clays Clay Miner.* **2017**, *65*, 104–121. [CrossRef]
16. Sandén, T.; Nilsson, U.; Andersson, L.; Svensson, D. ABM45 Experiment at Äspö Hard Rock Laboratory. Installation Report. SKB Rep. P-18-20. 2018. Available online: https://www.skb.com/publication/2491709/P-18-20.pdf (accessed on 1 June 2021).
17. Kaufhold, S.; Dohrmann, R. Mineralogical and Geochemical Alteration of the MX80 Bentonite from the LOT Experiment—Characterization of the A2 Parcel. Append. 7 SKB-TR-09-29. 2009. Available online: https://www.semanticscholar.org/paper/Mineralogical-and-geochemical-alteration-of-the-the/9005a2659c7419d96b1c81755b44a9a8f7067233 (accessed on 1 June 2021).
18. Olsson, S.; Karnland, O. Mineralogical and chemical characteristics of the bentonite in the A2 test parcel of the LOT field experiments at Äspö HRL, Sweden. *Phys. Chem. Earth* **2011**, *36*, 1545–1553. [CrossRef]
19. Dohrmann, R.; Olsson, S.; Kaufhold, S.; Sellin, P. Mineralogical investigations of the first package of the alternative buffer material test—II. Exchangeable cation population rearrangement. *Clay Miner.* **2013**, *48*, 215–233. [CrossRef]
20. Rousset, D.; Mosser-Ruck, R.; Cathelineau, M.; Villiéras, F.; Pelletier, M. Characterization of the LOT A2, 15 Test Parcel. Appendix 6 in SKB-TR-09-29. 2009. Available online: https://www.skb.com/publications/ (accessed on 1 June 2021).
21. Plötze, M.; Kahr, G.; Dohrmann, R.; Weber, H. Hydro-mechanical, geochemical and mineralogical characteristics of the bentonite buffer in a heater experiment. The HE-B project at the Mont Terri rock laboratory. *Phys. Chem. Earth* **2007**, *32*, 730–740. [CrossRef]
22. Fernandez, A.M.; Kaufhold, S.; Sánchez-Ledesmaa, D.M.; Reya, J.J.; Melóna, A.; Robredoa, L.M.; Fernándeza, S.; Labajoa, M.A.; Claveroa, M.A. Evolution of the THC conditions in the FEBEX in situ test after 18 years of experiment: Smectite crystallochemical modifications after interactions of the bentonite with a C-steel heater at 100 °C. *Appl. Geochem.* **2018**, *98*, 152–171. [CrossRef]
23. Kaufhold, S.; Dohrmann, R.; Degtjarev, A.; Koeniger, P.; Post, V. Mg and silica release in short-term dissolution tests in bentonites. *Appl. Clay Sci.* **2019**, *172*, 106–114. [CrossRef]
24. Kaufhold, S.; Dohrmann, R.; Ufer, K.; Kober, F. Interactions of bentonite with metal and concrete from the FEBEX experiment—mineralogical and geochemical investigations of selected sampling sites. *Clay Miner.* **2018**, *53*, 745–763. [CrossRef]
25. Karnland, O.; Olsson, S.; Nilsson, U. Experimentally determined swelling pressures and geochemical interactions of compacted Wyoming bentonite with highly alkaline solutions. *Phys. Chem. Earth* **2007**, *32*, 275–286. [CrossRef]
26. Martin, F.A.; Bataillon, C.; Schlegel, M.L. Corrosion of iron and low alloyed steel within a water saturated brick of clay under anaerobic deep geological disposal conditions: An integrated experiment. *J. Nucl. Mater.* **2008**, *379*, 80–90. [CrossRef]
27. Romaine, C.A.; Sabot, R.; Jeannin, M.; Necib, S.; Refait, P.H. Electrochemical synthesis and characterization of corrosion productson carbon steel under argillite layers in carbonated media at 80 °C. *Electrochim. Acta* **2013**, *114*, 152–158. [CrossRef]
28. El Mendili, Y.; Abdelouas, A.; Ait Chaou, A.; Bardeau, J.-F.; Schlegel, M.L. Carbon steel corrosion in clay-rich environment. *Corros. Sci.* **2014**, *88*, 56–65. [CrossRef]
29. Savoye, S.; Legrand, L.; Sagon, G.; Lecomte, S.; Chausse, A.; Messina, R.; Toulhoat, P. Experimental investigations on iron corrosion products formed in bicarbonate/carbonate containing solutions at 90 °C. *Corros. Sci.* **2001**, *43*, 2049–2064. [CrossRef]
30. Saheb, M.; Neff, D.; Demory, J.; Foy, E.; Dillmann, P. Characterisation of corrosion layers formed on ferrous archaeological artefacts buried in anoxic media. *Corros. Eng. Sci. Technol.* **2013**, *45*, 381–387. [CrossRef]